Available online at www.sciencedirect.com
SCIENCE DIRECT®
Applied Catalysis A: General 267 (2004) 203–216
APPLIED CATALYSIS A: GENERAL
www.elsevier.com/locate/apcata

Alumina-supported cobalt–molybdenum sulfide modified by tin via surface organometallic chemistry: application to the simultaneous hydrodesulfurization of thiophenic compounds and the hydrogenation of olefins

Jae-Soon Choi [a], Françoise Maugé [b], Christophe Pichon [a], Josette Olivier-Fourcade [c], Jean-Claude Jumas [c], Carine Petit-Clair [a], Denis Uzio [a,*]

[a] *IFP, Solaize BP No. 3, 69390 Vernaison, France*
[b] *Laboratoire Catalyse et Spectrochimie, UMR-CNRS 6506, ENSICaen, 6 Boulevard du Maréchal Juin, 14050 Caen Cedex, France*
[c] *Laboratoire des Agrégats Moléculaires et Matériaux Inorganiques, UMR-CNRS 5072, Place Eugène Bataillon, Case Courrier 015, 34095 Montpellier Cedex 5, France*

Received in revised form 25 February 2004; accepted 5 March 2004

Available online 9 April 2004

Abstract

Surface organometallic chemistry has been used to deposit tin atoms on an alumina-supported cobalt–molybdenum sulfide. The EXAFS spectra at the Mo and Co K-edges were not changed significantly by tin doping, which means that the initial morphology of sulfide phases was preserved during the synthesis. ^{119}Sn Mössbauer spectroscopy indicated that the main neighbors of the deposited tin atoms were sulfur and oxygen atoms with no significant formation of metallic tin particles. Tin seems thus to have been deposited either on the sulfide slabs through sulfur bridges or on the support via oxygen bonding. According to the infrared spectroscopy, tin doping led to the blocking of different surface sites with slight electronic structure modification. Those surface sites are sulfur vacancies on sulfide slabs, Al^{3+} or hydroxyl groups on the support, or "interfacial" sites: support hydroxyl groups H-bonded with sulfide phases.

The impact of tin doping on the activity and selectivity of the sulfide phases was studied by catalytic tests carried out using a synthetic FCC gasoline feed. Three main reactions were found to be involved: hydrodesulfurization of sulfur-containing molecules, double-bond isomerization and hydrogenation of olefins. Olefin hydrogenation was preceded by double-bond isomerization reaction, which gave quickly thermodynamically equilibrated composition. No clear correlation could be made between tin doping and isomerization performance and catalyst support was proposed as the main actor for this reaction. Small amounts of tin had little effect on the hydrogenation activity, but higher loadings resulted in an important decrease in activity. Contrary to the case of olefin hydrogenation, thiophene hydrodesulfurization activity decreased drastically at a low tin loading, and continued to decrease but more slightly at higher loadings. By comparison of the activity variations and the characterization results, the sulfur vacancies were found to play a major role in the hydrodesulfurization process. Interfacial sites were assumed to be involved in one of the key steps in the olefin hydrogenation pathway.

Keywords: Sulfides; $CoMo/Al_2O_3$; Tin doping; Surface organometallic chemistry; ^{119}Sn Mössbauer spectroscopy; FT-IR; CO chemisorption; Hydrodesulfurization; Olefin hydrogenation; Olefin isomerization; Selectivity

1. Introduction

Nowadays, the oil refining industry is faced to more and more stringent environmental legislation concerning the sulfur content in transportation fuels. In the European Union, for example, the sulfur content in gasoline will be reduced from 150 to 50 ppm in 2005 and maybe below 10 ppm in 2008 [1]. This drastic change in sulfur specifications is due to the negative effect of sulfur in gasoline on the function of catalytic converter, leading to increased automobile emissions such as nitrogen oxides (NO_x) and hydrocarbons [2]. These emissions are known as precursors of ozone in the troposphere [3].

* Corresponding author. Tel.: +33-4-78-02-29-06; fax: +33-4-78-02-20-66.
E-mail address: denis.uzio@ifp.fr (D. Uzio).

0926-860X/$ – see front matter © 2004 Elsevier B.V. All rights reserved.
doi:10.1016/j.apcata.2004.03.005

The gasoline pool is made up of products coming from various units in the refinery. In particular, it contains 20–40% of gasoline supplied by the fluid catalytic cracking unit (FCC gasoline) which has a high sulfur concentration (generally up to 2000 ppm). As FCC gasoline may represent alone more than 90% of the sulfur contained in a total gasoline pool, sulfur present in FCC gasoline is a key target in order to meet future sulfur specifications on gasoline. One of the viable technological options is the hydrodesulfurization (HDS) of FCC gasoline [4,5].

Main sulfur compounds present in FCC gasoline are thiophenes and benzothiophenes and they are relatively easy to remove by conventional HDS catalysts [6,7]. However, a major technical problem encountered with conventional catalysts is that desulfurization is accompanied by the hydrogenation (HYD) of olefins, which are also abundantly (25–50%) present in FCC gasoline. Olefin saturation through hydrogenation leads to a considerable loss of octane number [8].

Many research efforts have thus been made to increase the selectivity (HDS/HYD) of the conventional sulfide-based catalysts (e.g., $CoMo/Al_2O_3$) by modifying their composition or surface properties: deactivated $CoMo/Al_2O_3$ sulfides (used or pretreated by coking) [9–12], use of basic organic compounds like pyridines [13,14], or promotion by basic support [15–17]. Nevertheless, contradictory results still exist in the field of the improvement of the HDS/HYD selectivity, showing that fundamental knowledge is still needed to explain the phenomena.

While edge sites of sulfide slabs are generally accepted as active sites of sulfided $CoMo/Al_2O_3$ [7,18–20], their detailed local structures and catalytic roles are still not clearly elucidated. For example, despite the arguments in favor of the same sites for HDS and HYD [17], there are also various evidences supporting models with different sites. It is well known, indeed, that HDS activity is highly promoted by the addition of Co to Mo sulfide, while little or negative effect is observed on olefin HYD [21–24]. Moreover, hydrogen sulfide (H_2S) inhibits HDS and straight-chain olefin HYD [23,25] but does promote branched-chain olefin HYD [23]. It is also remarkable that thiophene HDS/butene HYD selectivity increases when the active phase of a $CoMo/Al_2O_3$ catalyst is transformed from the so-called Type I Co–Mo–S structure into Type II Co–Mo–S by increasing the sulfidation temperature [26].

In this respect, it is of first importance to improve preparation method in order to realize meaningful structure–reactivity studies on well-defined catalysts [7]. Classical impregnation methods does not seem well suited for this purpose, because the insertion of a promoter requires subsequent thermal treatments at elevated temperatures (drying, calcination, or re-sulfidation), and this may result in significant bulk structure modifications (e.g., sintering or modification of the promotion level).

Surface organometallic chemistry (SOMC) has shown a high potential for the preparation of supported bimetallic catalysts with desired composition and structure [27]. For example, the successive hydrogenolysis of tetra-*n*-butyltin ($Sn(n\text{-}C_4H_9)_4$) on the surface of group VIII metals leads to a well-defined bimetallic catalyst supported on an oxide [27–30]. In SOMC on oxide-supported metals, a complete selection of reaction conditions (temperature, initial complex concentration, etc.) allows the reaction to occur preferentially between organometallic compounds and metal surfaces [27,29,30].

Similar attempts have been made for the preparation of mixed transition-metal sulfides [31–34]. These studies showed that promotion by cobalt or nickel is more efficient by reaction between pre-sulfided molybdenum (or tungsten sulfides) and promoter-containing organometallic complexes than by conventional impregnation. However, hardly any information has been reported about the chemistry involved during the catalyst preparation. Recently, we applied the SOMC method to the modification of alumina-supported (Co)Mo sulfides by cobalt or tin [24]. As in the case of metallic catalysts, successive hydrogenolysis was found to be involved in the SOMC modification of sulfide catalysts. Moreover, the surface morphology of the initial sulfide was preserved without significant Sn particle formation. The content of fixed Sn was found to reach a plateau, indicating the adsorption type of the surface reaction by the SOMC method.

The objective of the present work was to obtain comprehensive information about the mechanism of hydrodesulfurization and olefin hydrogenation over sulfides and to get a better insight into relationship between different sites and catalyst selectivity (HDS/HYD). Tin was added to sulfided $CoMo/Al_2O_3$ and the resulting reactivity variations were studied. The SOMC method was used for tin deposition and the local structure of Sn on sulfided $CoMo/Al_2O_3$ was characterized by a multi-technique approach consisting of ^{119}Sn Mössbauer and infrared spectroscopies, as well as EXAFS.

2. Experimental

2.1. Preparation of the catalysts

Modification of CoMo sulfides using SOMC was carried out by reacting tetraallyltin ($Sn(C_3H_5)_4$, +95%, Strem Chemicals) with the surface of freshly sulfided $CoMo/Al_2O_3$. Tetraallyltin was preferred to tetra-*n*-butyltin because of its higher reactivity towards the surface [24]. First, an oxide precursor (3 wt.% CoO−10 wt.% MoO_3/Al_2O_3) was sulfided in flowing 15 vol.% H_2S/H_2 under atmospheric pressure. The pre-sulfidation temperature was raised from room temperature (RT) to 673 K at 300 K h^{-1} and maintained for 2 h. Then the temperature was lowered to 473 at 300 K h^{-1}. At this temperature the gas flow was switched to pure H_2 and the reaction was further maintained for 2 h. Then, the reactor was rapidly cooled to RT in flowing H_2 and finally pulses of 15 vol.%

H_2S/H_2 were injected until the saturation of the surface sites occurred. The as-prepared sulfide was then transferred, without air contact, to the reactor designed for the SOMC treatment. This reactor, containing the solution (complex + solvent), had been purged by Ar flow before catalyst introduction. The reaction was done at RT in flowing H_2 for 2 h. After reaction, the catalyst was washed with pure solvent (*n*-heptane) under Ar flow. To ensure complete decomposition of the anchored complexes, a post-treatment was performed by reduction under pure H_2 flow at 473 K. The resulting materials were ground into fine powder and then stocked under Ar atmosphere to avoid any contact with air before catalyst characterization.

2.2. Characterization

^{119}Sn Mössbauer spectroscopy analyses were carried out at RT using an EG&G Novelec constant acceleration spectrometer in transmission mode. The source of γ-rays was ^{119m}Sn in a $BaSnO_3$ matrix with a nominal activity of 10 mCi. The velocity scale was calibrated with the magnetic sextet of a high purity iron foil absorber, using ^{57}Co(Rh) as source. A fresh Sn-containing sample was placed in the specific Pyrex cell, which was sealed under vacuum and then transferred to the spectrometer. The Mössbauer spectroscopy analyses were thus realized without any contact of the powered samples with air. The recorded spectra were fitted with Lorentzian profiles by a least-squares method [35]. The isomer shifts were determined relative to the center of the $BaSnO_3$ spectrum recorded at RT.

For the infrared (IR) spectroscopy measurements, the sulfide sample previously kept under Ar was taken out in air and pressed into a self-supporting disc (10 mg, 2 cm^2). It was then placed into the IR cell and re-sulfided in situ under the same conditions as those used for the initial sulfidation. The main difference was that, after the reduction procedure, the IR cell was evacuated during the temperature decrease from 473 K to RT and no H_2S/H_2 pulse was injected. First, IR spectra of fresh sulfide were obtained at RT and 100 K, then small calibrated pulses of carbon monoxide (CO) were introduced into the IR cell at 100 K up to an equilibrium pressure of 133 Pa. IR spectra were recorded after each CO introduction with a Nicolet Magna 550 FT-IR spectrometer equipped with a liquid-nitrogen-cooled MCT detector. The spectrometer operated at 4 cm^{-1} resolution collecting 512 scans.

X-ray absorption experiments were performed at LURE (Laboratoire pour l'Utilisation du Rayonnement Electromagnétique, Orsay, France) using DCI, a storage ring operated with an electron energy of 1.85 GeV and a current between 260 and 360 mA. Data were collected at RT on the EXAFS IV station, which is equipped with a Si (4 0 0) double crystal monochromator for the Mo K-edge (20 000 eV), and a double borosilicate mirror for the rejection of harmonics. Measurements were done in transmission mode using ionization chambers filled with argon to absorb around 20% of the X-ray beam in the first ion chamber and the remainder in the second ion chamber. At the Mo K-edge, each spectrum was recorded three times with a step of 3 eV (from 19 900 to 21 000 eV) and 2 s per point. The energy/angle calibration was performed using Co, Mo, or Sn foil as reference. After sieving, particles in the 100–200 μm range were loaded into a sample holder sealed by self-adhesive Kapton® tape that is transparent to the X-ray beam. The loading of the sample holder was performed in a glove box filled with pure nitrogen to avoid oxidation of the sample. The Mo K-edge was recorded with a sample thickness of 4 mm. Normalized EXAFS spectra were isolated from the experimental data using standard procedure [36]. Data analysis was performed by using the "EXAFS pour le Mac" package [37]. Fourier transforms (FTs) of the k^3-weighted EXAFS functions were obtained using a Kaiser type window ranging from 4.08 to 16.17 $Å^{-1}$ beyond the Mo K-edge. In this work, FTs were calculated and presented without phase correction. The inverse Fourier transforms (FT^{-1}s or filtered EXAFS) were obtained in the range between 1.42 and 3.30 Å for Mo. Two filtered EXAFS spectra per sample were calculated: one per each peak on the FT (the first one is obtained in the range between 1.42 and 2.39 Å; the second one in the range between 2.42 and 3.30 Å). Theoretical amplitudes and phase functions for all the possible bonds in the material involving a Mo atom were calculated using FEFF 8.10 software [38]. The structural parameters (inter-atomic distances) of the calculated references used in this study are summarized in Table 1. A one- or two-shell least-squares fitting procedure (in *k*-space) using a single scattering EXAFS formulation was employed to extract, from each filtered EXAFS spectra, the coordination number (*N*), inter-atomic distance (*R*), and Debye–Waller factor (σ) with Round Midnight software [37].

Table 1
Inter-atomic distances of the reference shells

Shell	Distance (Å)
Mo–Co	3.3
Mo–Mo	3.3
Mo–S	2.4

2.3. Catalytic tests

Catalytic performance of the prepared sulfides was evaluated in an autoclave under constant hydrogen pressure with a model FCC gasoline feed. This feed was composed of 1000 ppm sulfur as 3-methylthiophene (>98%, Fluka), 10 wt.% olefin as 2,3-dimethyl-2-butene (>97%, Fluka) or 1-hexene (∼98%, Fluka), and solvent as *n*-heptane (>99%, HPLC grade, Fluka). Fresh catalyst was introduced under argon (Ar) flow into the reactor containing *n*-heptane, which was also previously purged by Ar flow to prevent any air contact of the catalyst. The reactor was purged again by nitrogen (N_2) stream, prior to the injection of reactants consisting of 3-methylthiophene (3-MT) and 2,3-dimethyl-2-butene

(2,3-DMB2N) or 1-hexene (H1N). Then, the temperature was increased up to the reaction temperature of 473 K under N_2 atmosphere. After introducing hydrogen (H_2) to have a total reaction pressure of 2.5 MPa, the reaction was started by stirring the reaction mixture. Under these reaction conditions, the absence of mass transport limitation was checked by a linear increase of the reaction rate with increasing the mass of the catalyst. The composition of the reaction mixture was monitored during the reaction, by analyzing the liquid samples using a gas chromatograph (Varian, CP-3800) equipped with a flame ionization detector and a 50 m long and 0.2 mm diameter (i.d.) capillary column (HP PONA, 0.5 μm film thickness).

3. Results

3.1. Tin doping of $CoMo/Al_2O_3$ sulfide by SOMC

As described in Section 2, the tin doping proceeded in two steps: liquid phase reaction of the organometallic complexes ($Sn(C_3H_5)_4$) and the sulfide catalyst (*anchoring*), followed by thermal decomposition of the surface organometallic complexes (*grafting*). More detailed information about the mechanism of SOMC tin doping of a sulfide catalyst are given elsewhere [24] and we summarize hereafter the major results to facilitate the following interpretation of characterization data.

The tin complex adsorbs on the surface of the solid via an adsorption equilibrium process, the loading reaches a plateau for high concentration of tin precursor in the solution. The gas analyzed during the Sn adsorption was mainly propene with some traces of propane and the quantity of gas produced was almost equal for anchoring and grafting steps. Moreover, up to 90% of the carbon in the Sn complexes was removed during the anchoring and grafting. From these observations, it can be concluded that a preferential hydrogenolysis of the C–Sn bond was involved in the anchoring and grafting of the Sn complexes. First, two allyl ligands of a $Sn(C_3H_5)_4$ complex were removed as propene, forming a surface tin complex. Then, the thermal post-treatment further hydrogenolyzed the remaining two ligands, leaving on the catalyst surface nearly ligand-free Sn.

3.2. ^{119}Sn Mössbauer spectroscopy

Fig. 1 presents the ^{119}Sn Mössbauer spectra of sulfided $CoMo/Al_2O_3$ with different Sn contents. For a better interpretation of the spectra, reference samples obtained by the SOMC between tin complexes and pure alumina support were also studied. Different Sn/Al_2O_3 samples were prepared by changing the mode of pre- or post-treatments (Fig. 2). The corresponding spectroscopic data are summarized in Tables 2 and 3.

The identification of the Mössbauer data was performed using the scale of isomeric shifts obtained from some reference Sn compounds available at the Laboratoire des

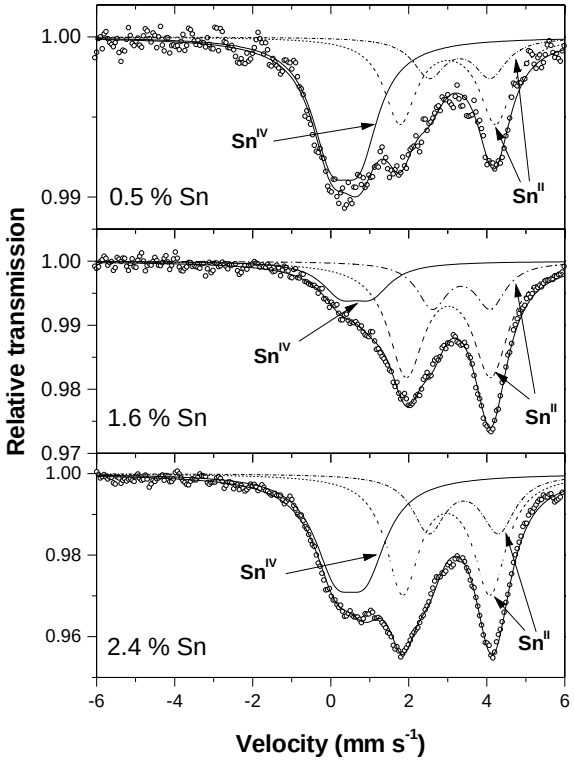

Fig. 1. ^{119}Sn Mössbauer spectra of Sn-doped $CoMo/Al_2O_3$ sulfides.

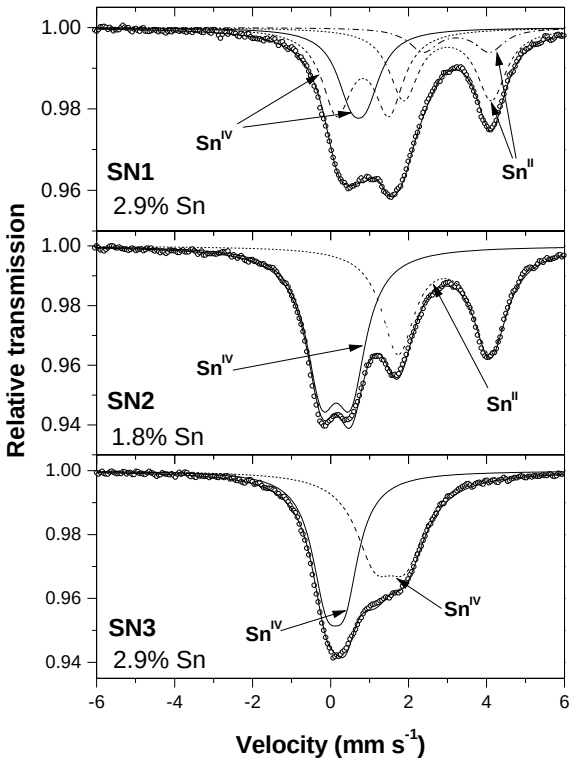

Fig. 2. ^{119}Sn Mössbauer spectra of Sn/Al_2O_3 with different treatments. SN1: pre-sulfidation of alumina at 673 K and reduction at 473 K of SOMC-treated sample; SN2: pre-drying of alumina at 393 K and reduction at 473 K of SOMC-treated sample; SN3: pre-sulfidation of alumina at 673 K and drying at RT of SOMC-treated sample.

Table 2
^{119}Sn Mössbauer spectroscopic data on $CoMo/Al_2O_3$ sulfides with 0.5–2.4 wt.% Sn

Sample	Isomer shift (mm s^{-1})	Quadrupole splitting (mm s^{-1})	Species	Molar percentage
0.5% Sn–$CoMo/Al_2O_3$	0.26 (3)	0.73 (3)	Sn(IV)	49.4
	2.89 (5)	2.45 (7)	Sn(II)	34.8
	3.20 (11)	1.57 (14)	Sn(II)	15.8
1.6% Sn–$CoMo/Al_2O_3$	0.56 (2)	0.79 (4)	Sn(IV)	17.2
	2.91 (1)	2.17 (1)	Sn(II)	61.7
	3.24 (1)	1.49 (2)	Sn(II)	21.1
2.4% Sn–$CoMo/Al_2O_3$	0.40 (2)	0.78 (2)	Sn(IV)	37.6
	2.86 (2)	2.24 (2)	Sn(II)	42.1
	3.30 (3)	1.79 (4)	Sn(II)	20.3

Table 3
^{119}Sn Mössbauer spectroscopic data on Sn/Al_2O_3 with different treatments

Sample code	Sn content (%)	Isomer shift (mm s^{-1})	Quadrupole splitting (mm s^{-1})	Species	Molar percentage
SN1[a]	2.9	0.61 (1)	0.39 (2)	Sn(IV)	23.6
		0.72 (1)	1.34 (1)	Sn(IV)	35.4
		2.89 (2)	2.25 (3)	Sn(II)	30.9
		3.21 (6)	1.70 (7)	Sn(II)	10.1
SN2[b]	1.8	0.03 (1)	0.75 (1)	Sn(IV)	53.2
		2.80 (1)	2.36 (1)	Sn(II)	46.8
SN3[c]	2.9	0.01 (1)	0.48 (1)	Sn(IV)	49.3
		1.42 (1)	0.79 (1)	Sn(IV)	50.7

[a] Pre-sulfidation of alumina at 673 K and reduction at 473 K of SOMC-treated sample.
[b] Pre-drying of alumina at 393 K and reduction at 473 K of SOMC-treated sample.
[c] Pre-sulfidation of alumina at 673 K and drying at RT of SOMC-treated sample.

Agrégats Moléculaires et Matériaux Inorganiques (LAMMI, Montpellier) (Fig. 3). The Sn/Al_2O_3 sample, prepared under the same conditions as the Sn-doped $CoMo/Al_2O_3$ (SN1 in Fig. 2 and Table 3), had two oxidation states (IV and II). Two different Sn species were obtained for each oxidation state by peak decomposition. The observed Sn^{IV} peaks (0.61 and 0.71 mm s^{-1}) probably correspond to Sn oxysulfide species. One of the Sn^{II} species shows an isomeric shift characteristic of a stannous oxide (2.89 mm s^{-1}), whereas the other species might be due to an oxysulfide or sulfide (3.21 mm s^{-1}). These ascriptions were confirmed by the results on sample SN2, the alumina of which was simply dried at 393 K instead of pre-sulfidation before SOMC treatment.

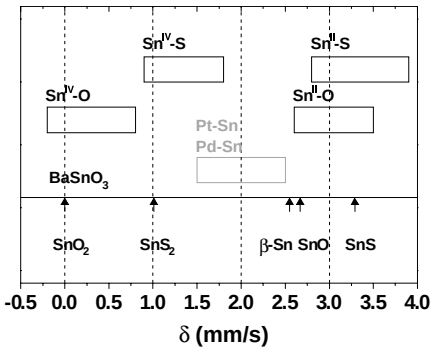

Fig. 3. Scale of isomeric shifts for tin.

In this case, two species were clearly identified, Sn^{IV} stannic oxide (near SnO_2) and Sn^{II} stannous oxide (near SnO). The SN3 sample was prepared with pre-sulfided alumina but the sample was simply dried at RT after the anchoring of the Sn complexes. This sample showed only Sn^{IV} species: one oxide species (SnO_2 type) and one covalent species, probably due to the residual hydrocarbon ligands on Sn atoms.

The $CoMo/Al_2O_3$ sulfides with different Sn loadings contain the same Sn species, but with different proportions (Fig. 1 and Table 2). The Sn^{IV} was ascribed to intermediate species between two Sn^{IV} species of Sn/Al_2O_3. However, the larger peak width (1.2–1.3 mm s^{-1}) suggests that both Sn^{IV} species were also present on the sulfided $CoMo/Al_2O_3$. Practically, the same types of Sn^{II} species (one oxide and one (oxy)sulfide) were found on sulfided $CoMo/Al_2O_3$ and Sn/Al_2O_3 (SN1).

3.3. Infrared spectroscopy

IR spectroscopy was used to investigate the different surface sites, either by studying chemisorbed CO (Figs. 4 and 5), or by monitoring directly the surface OH groups (Figs. 6 and 7) on the sulfided catalysts. The infrared spectrum of CO (IR(CO)) adsorbed at 100 K on sulfided $CoMo/Al_2O_3$ without Sn doping (Fig. 4), corresponds to typical IR(CO) spectra obtained on sulfided $CoMo/Al_2O_3$ [21,31,39] with principally four different types of CO

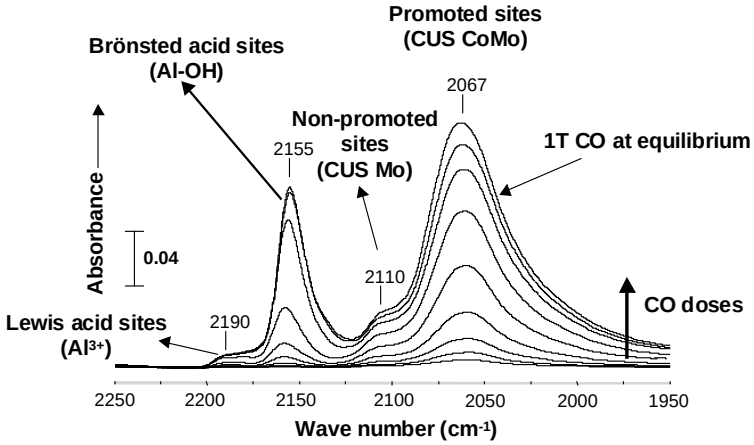

Fig. 4. IR spectra of CO species resulting from the introduction of increasing doses of CO at 100 K on a reference sulfided $CoMo/Al_2O_3$.

species. First, two characteristic bands of CO on alumina could be observed. The bands at 2155 and 2190 cm^{-1} correspond, respectively, to CO hydrogen-bonded to hydroxyl groups (Brønsted acid sites) [31,40,41] and to CO coordinated to the Lewis acid sites of alumina (Al^{3+}) [31,40–43]. The lower wave number region is characteristic of sulfide phases: CO chemisorbed on coordinately unsaturated sites (CUS). The band at 2067 cm^{-1} is due to the Co-promoted Mo sulfide sites [17,21,31]. The shoulder around 2055 cm^{-1} could indicate the presence of Co that is not connected with Mo sites [31,39]. The band at 2110 cm^{-1}, characteristic of non-promoted Mo sites [21,31,39,41,43,44], has a very weak intensity. It means that almost all Mo edge sites are in interaction with Co atoms evidencing the good promotion level of this sulfided catalyst. The spectra of the tin-doped catalysts display the same kind of bands as the reference sulfided $CoMo/Al_2O_3$, but Sn led to a decrease of the band intensity (Fig. 5a). No significant band shift could be noted with Sn loading, except maybe small decrease in wave number (2–3 cm^{-1}) for samples with high Sn loadings. The evolution of the band intensity with Sn loading is reported in Fig. 5b for the different CO species. The contributions of CO chemisorbed on non-promoted and Co-promoted sites were combined to the total CUS on the sulfide phases.

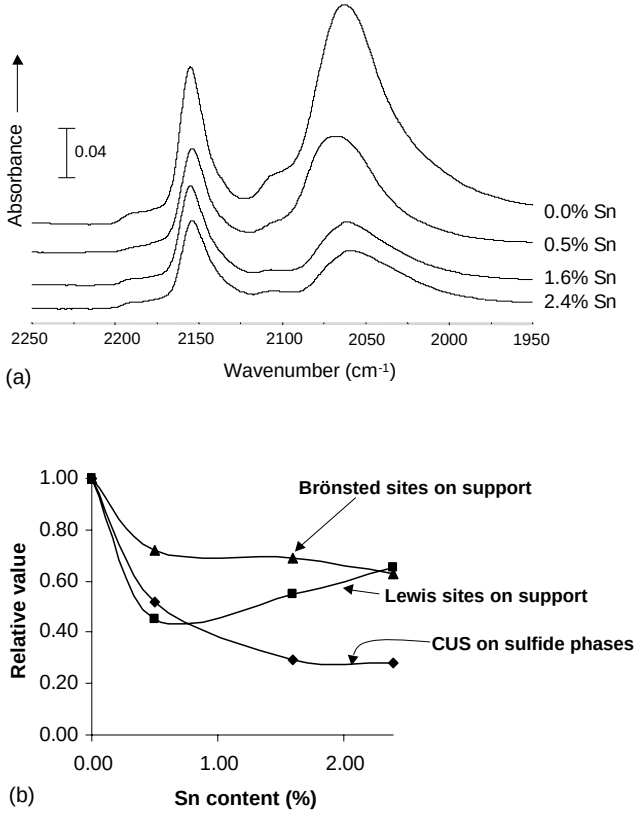

Fig. 5. (a) Evolution of IR spectrum of chemisorbed CO at 100 K, with increasing Sn loading on sulfided $CoMo/Al_2O_3$ and (b) relative absorbance values of different CO species vs. Sn loading.

On the other hand, the OH groups of the alumina support were also directly monitored at RT before CO introduction (Fig. 6). Sulfided alumina showed two bands at 3731 and 3681 cm^{-1} specific of acidic OH groups as well as a broad band characteristic of H-bonded OH groups (Fig. 6a). This points out the high hydroxylation degree of the alumina surface in agreement with the low temperature of final evacuation (473 K). Deposition of Sn by SOMC on pure alumina decreased only slightly the number of OH groups and no preferential interaction can be noticed (Fig. 6a).

On the sulfided $CoMo/Al_2O_3$ samples, a decrease of the alumina OH groups is observed in agreement with the support coverage by the sulfided phase (Fig. 6b). This decrease is more important on Sn-containing catalysts. To better evaluate the modifications in the OH group zone, the spectrum of the sulfided alumina was subtracted from those of the sulfided CoMo catalysts (Fig. 7). For the sulfided $CoMo/Al_2O_3$, the negative bands at 3731 and 3681 cm^{-1} confirm the decrease of the number of free-alumina OH groups in presence of sulfided phase. The positive band at 3630 cm^{-1} points out the appearance of support OH groups perturbed by the presence of the sulfided phase [45–48], these OH groups will be called “interfacial sites” in the following. Such sites

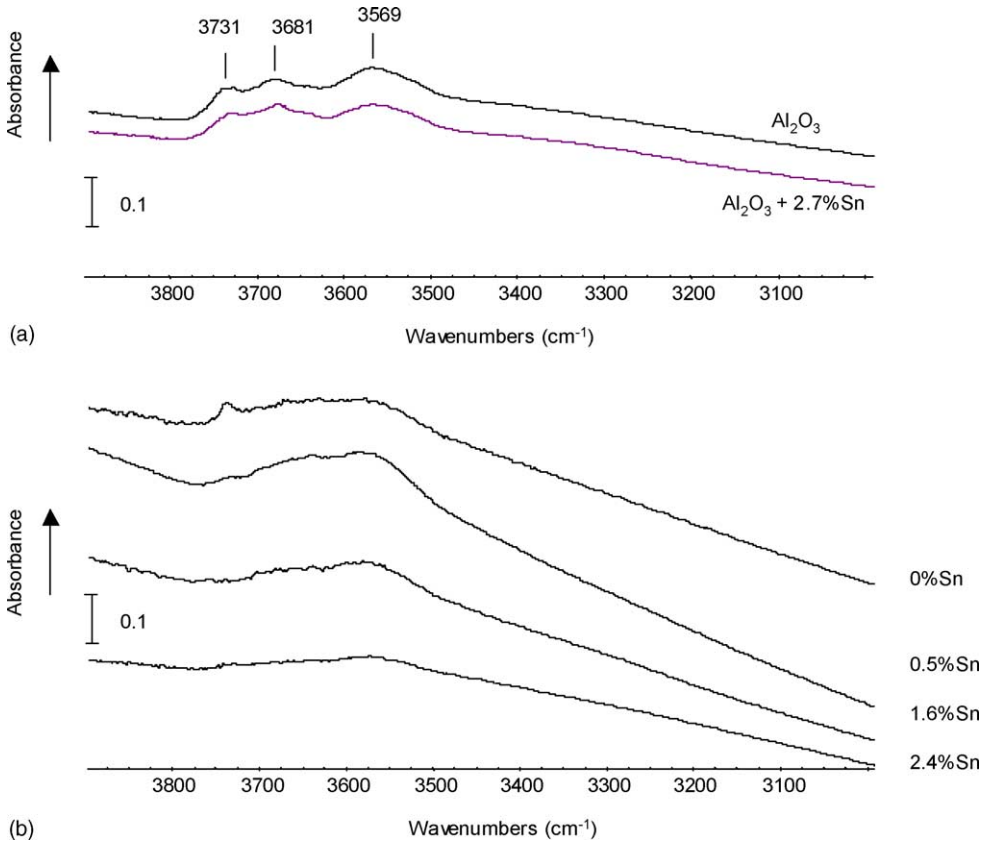

Fig. 6. IR spectra of the OH band region of the (a) sulfided Al_2O_3 support with and without 2.7% Sn and (b) sulfided $CoMo/Al_2O_3$ with different Sn loadings.

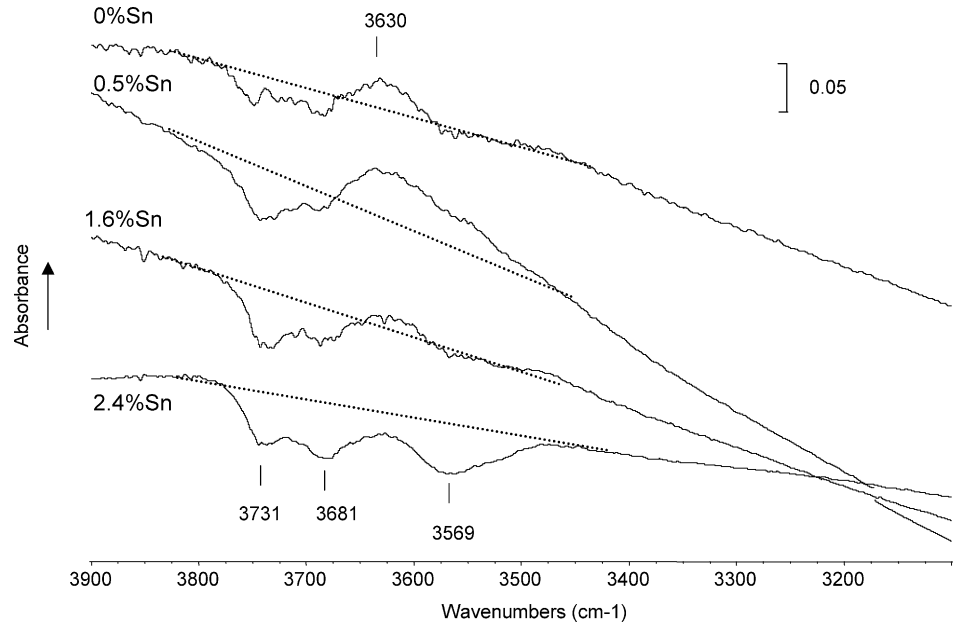

Fig. 7. IR spectra of the OH band region of the sulfided $CoMo/Al_2O_3$ with different Sn loadings, after subtraction of sulfided alumina contribution.

could correspond to acidic alumina OH groups in interaction with basic sites of the sulfided phase (such as sulfur ions or SH groups). Until 1.6% Sn, Sn deposition leads more specifically to a decrease of the high wave number alumina OH groups while for the highest amount of Sn introduced, H-bonded hydroxyls groups (band at 3569 cm^{-1}) are strongly affected. Variation of the acidic OH groups (bands at 3731 and 3681 cm^{-1}) is consistent with the IR(CO) re-

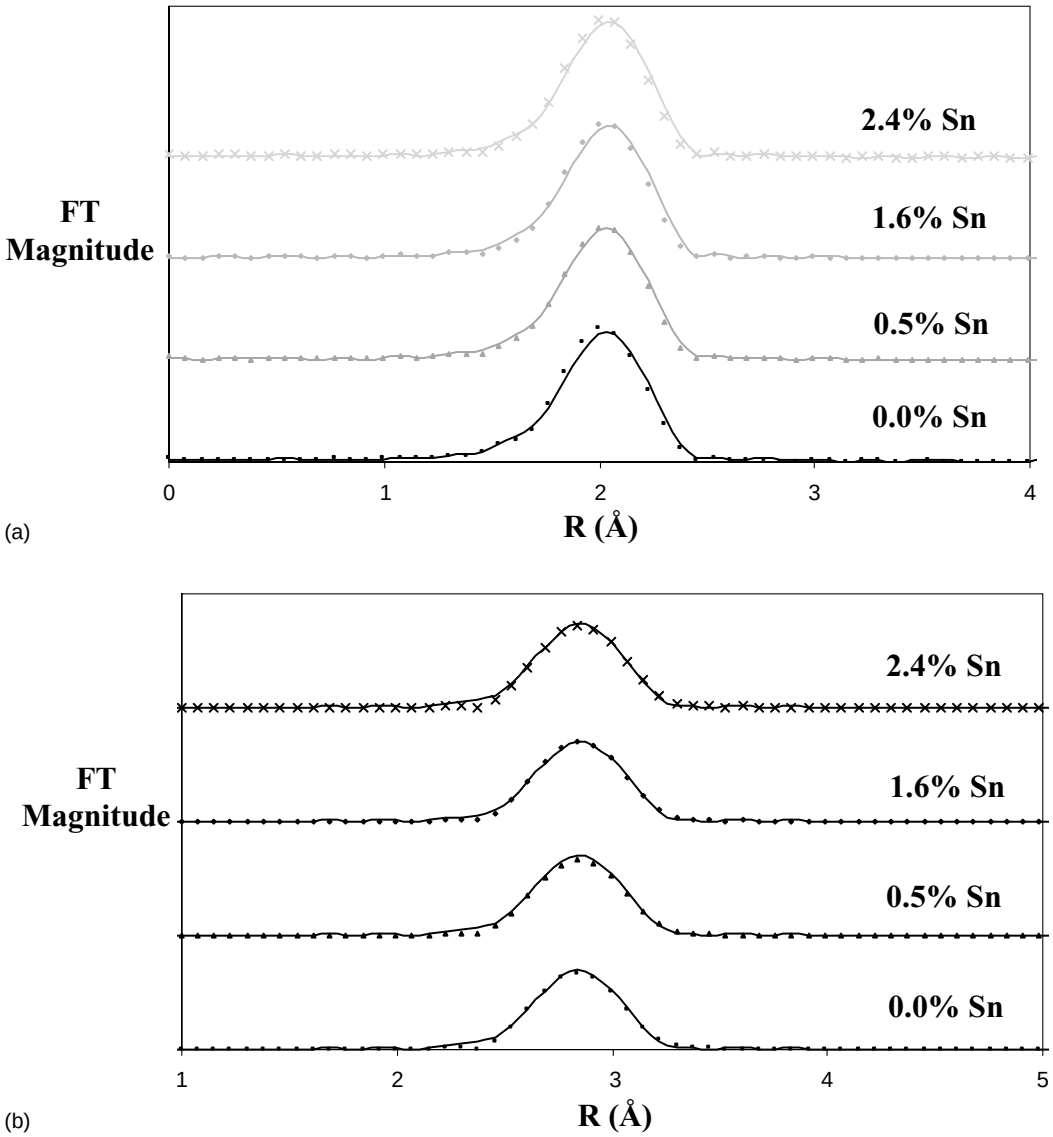

Fig. 8. Experimental and calculated Fourier transforms ((a) first peak and (b) second peak) of the EXAFS spectra at the Mo K-edge of Sn-doped $CoMo/Al_2O_3$ sulfides (0–2.4 wt.%). Dotted lines and solid lines represent experimental (filtered) and calculated spectra, respectively.

sults. Additionally, a higher Sn loading (1.6 and 2.4% Sn) induces a diminution of the band at 3630 cm^{-1} although the simultaneous decrease of alumina H-bonded OH groups prevent a clear following of the intensity variation of the "interfacial site" band.

3.4. EXAFS

Whatever the content of doped Sn (0–2.4 wt.%), the spectra looked quite similar for a given edge. As an example, Fig. 8 shows experimental and calculated Fourier transforms of the EXAFS spectra obtained at the Mo K-edge. The results of the numerical simulation, for the Mo K-edge, in terms of global and specific (structural) parameters, are reported in Table 4. Note that the numerical simulation gave a typical residual in the order of 10^{-2}. Also note that the adjustable parameter related with energy origin (ΔE_0) was constrained to be the same for each shell of a given least-squares fitting. According to the fitted data (Table 4), the reference sample (0 wt.% Sn) showed the coordination distances and numbers of Mo–S, Mo–Mo shells comparable to previously reported results on $CoMo/Al_2O_3$ sulfides [17,49–51]. However, the coordination distance of Co–Mo (3.23 Å) was substantially higher than the usually reported value (2.80 Å).

3.5. Catalytic test with the feed containing 3-methylthiophene and 2,3-dimethyl-2-butene

Fig. 9 shows a typical plot of conversion versus reaction time obtained over the different sulfide catalysts studied.

Table 4
EXAFS analysis of Sn-doped $CoMo/Al_2O_3$ sulfides (0–2.4 wt.%) at the Mo K-edge

Sn content (%)	Shell	N[a]	R (Å)[b]	$\Delta\sigma$ (Å)	ΔE_0 (eV)
0.0	Mo–S	5.3	2.41	0.064	6.7
	Mo–Mo	2.5	3.16	0.069	−1.5[c]
	Mo–Co	1.1	3.23	0.062	−1.5[c]
0.5	Mo–S	5.4	2.41	0.063	7.5
	Mo–Mo	2.4	3.15	0.069	−1.0[d]
	Mo–Co	1.2	3.22	0.066	−1.0[d]
1.6	Mo–S	5.5	2.42	0.065	9.0
	Mo–Mo	2.1	3.15	0.069	−1.0[e]
	Mo–Co	1.5	3.25	0.066	−1.0[e]
2.4	Mo–S	5.5	2.41	0.064	9.0
	Mo–Mo	2.2	3.19	0.070	−1.0[f]
	Mo–Co	0.6	3.25	0.066	−1.0[f]

[a] ±0.5.
[b] ±0.05.
[c,d,e,f] Constrained to be equal.

For the total conversion of 3-methylthiophene, a first-order kinetic law, resulting in a good fit of the experimental data, was used to compare the HDS activities of different catalysts in this study. In the reaction products, some 3-methyltetrahydrothiophene, thiols and alkylthiophenes other than 3-MT were detected. However, the contribution of these products was estimated to be negligible under our test conditions. In the case of 2,3-dimethyl-2-butene, an important conversion had already been made during the heating of the reaction mixture under N_2 (Fig. 9). During the reaction under H_2 pressure, the rate of olefin conversion slowed down with reaction time and became constant at ca. 30 min. This rather complex kinetic behavior was, in fact, due to the concomitant presence of isomerization and hydrogenation reactions. Indeed, during the heating of the reaction mixture under N_2 and at the beginning of the reaction under H_2, only isomerization of 2,3-DMB2N to 2,3-dimethyl-1-butene (2,3-DMB1N) took place (Fig. 10a) and hydrogenation reaction to 2,3-dimethylbutane (2,3-DMBN) began only when the ratio 2,3-DMB1N/2,3-DMB2N became constant

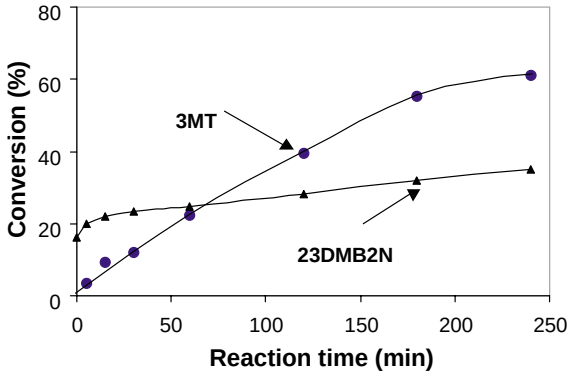

Fig. 9. Conversion of 3-methylthiophene and 2,3-dimethyl-2-butene as a function of reaction time over a reference $CoMo/Al_2O_3$ sulfide catalyst.

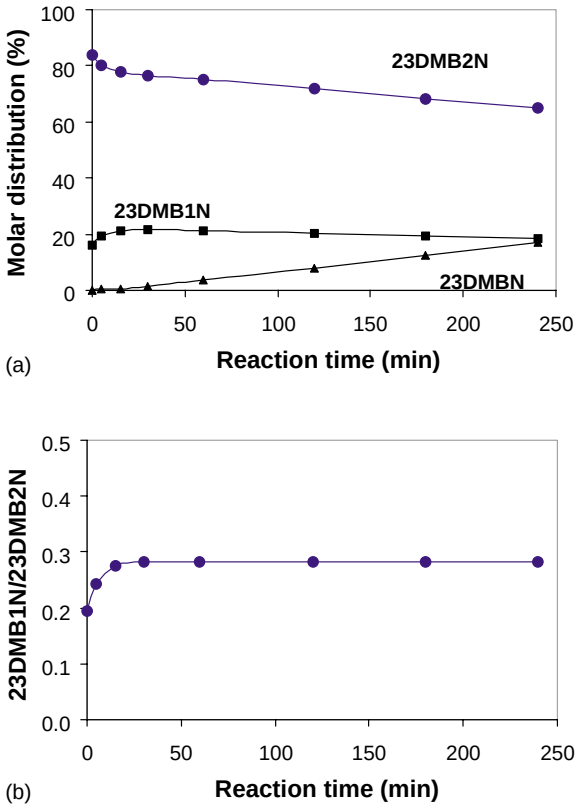

Fig. 10. (a) Molar distribution of products from 2,3-dimethyl-2-butene conversion as a function of reaction time and (b) evolution of molar ratio of 2,3-dimethyl-1-butene to 2,3-dimethyl-2-butene with reaction time.

(Fig. 10a and b). Hydrogenation reaction was nicely fitted with zero-order kinetic laws.

3.6. Catalytic test with the feed containing 3-methylthiophene and 1-hexene

The conversion of 3-MT showed again apparent first-order kinetics (Fig. 11). A significant H1N conversion was observed as a result of heating under N_2 atmosphere. Then the conversion increased rapidly up to near 100% during the reaction under H_2 pressure and stabilized at ca. 1 h of reac-

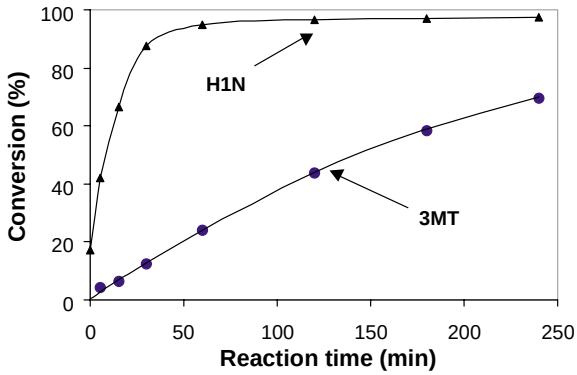

Fig. 11. Conversion of 3-methylthiophene and 1-hexene as a function of reaction time over a reference $CoMo/Al_2O_3$ sulfide catalyst.

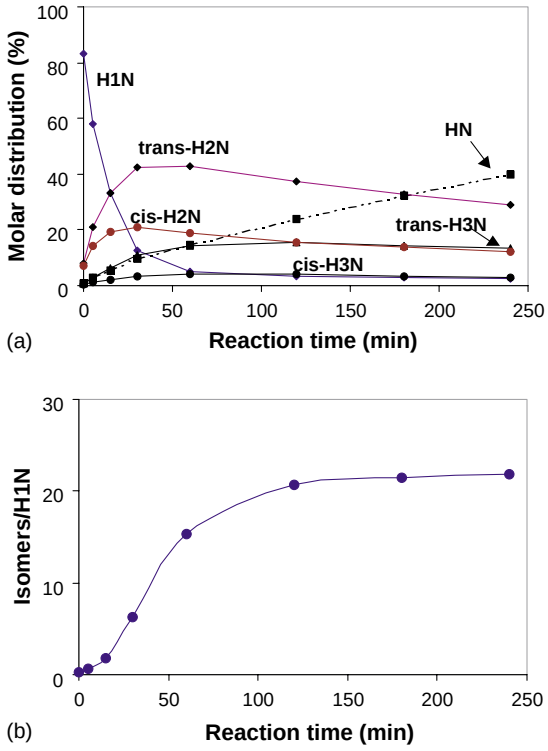

Fig. 12. (a) Molar distribution of products from 1-hexene conversion as a function of reaction time and (b) evolution of molar ratio of 1-hexene to 2-hexenes (H2N) plus 3-hexenes (H3N) with reaction time.

tion time. H1N isomerization prevailed at the beginning of the reaction but hydrogenation was also present (Fig. 12a), unlike the test with 2,3-DMB2N. When increasing reaction time, the isomers approached their equilibrium composition and hexane (HN) formation by hydrogenation showed apparent zero-order kinetics (Fig. 12a and b). For the first 1 h of reaction, hydrogenation deviated a little from zero-order behavior. As a consequence, HYD rate constants were calculated, for comparison, from the data obtained for the reaction time higher than 1 h.

3.7. Influence of Sn doping on the catalytic performance

This part compares the activities of catalysts with various tin loadings, for the three main reactions involved: isomerization, hydrogenation and hydrodesulfurization. Due to a considerable isomer formation during the heating of the feed in N_2, no meaningful kinetic analysis was possible for the olefin isomerization. Thus, a direct comparison of reaction curves (H1N isomerization versus reaction time) was made for the comparison of isomerization activities (Fig. 13). In general, all catalysts showed similar behavior and tin doping did not seem to have significant impact on isomerization performance. However, some discrepancy could be noted at the beginning of the reaction without however apparent correlation with loaded tin content. Unlike ISOM, tin doping resulted in remarkable activity changes in both HDS and HYD, as indicated by Fig. 14 where activities are presented

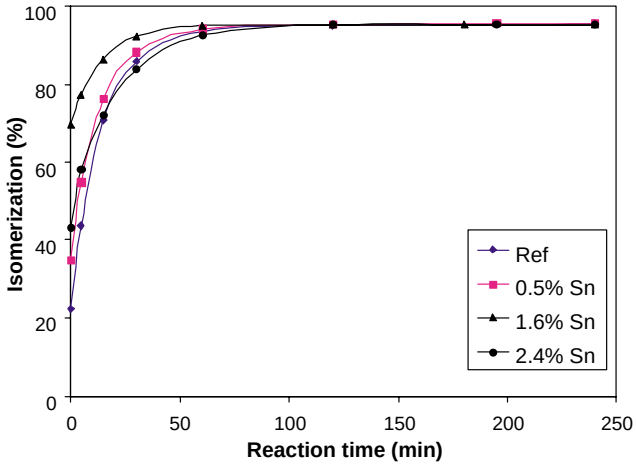

Fig. 13. Comparison of the performance of $CoMo/Al_2O_3$ catalysts with different Sn loadings (0–2.4 wt.%), for 1-hexene isomerization in the presence of 3-methylthiophene.

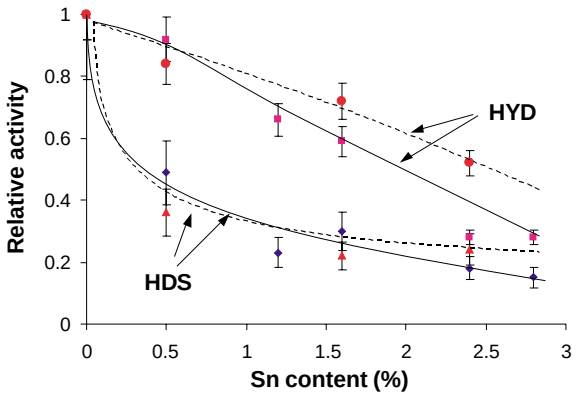

Fig. 14. Evolution of 3-methylthiophene HDS and olefin HYD activities as a function of Sn loadings. Dashed lines correspond to the mixture of 3-MT and 2,3-dimethyl-2-butene and solid lines to that of 3-methylthiophene and 1-hexene.

relative to the activities of reference catalyst. With increasing loading, tin doping suppressed gradually both HDS and HYD reactions. However, the decrease trend was clearly different for these two reactions. A small dose of Sn (0.5 wt.%) diminished drastically HDS and HDS activity continued to decrease with increasing Sn loading although to a much lesser extent. In the case of HYD, 0.5 wt.% of Sn showed little effect and activity decrease became important at higher Sn loadings. Moreover, the activity decrease of 2,3-DMB2N HYD was less important than that of H1N HYD with Sn doping.

4. Discussion

4.1. Tin deposition on $CoMo/Al_2O_3$ sulfide via SOMC

Mössbauer spectroscopy showed that the tin environment was rich in sulfur and oxygen, their proportion depending

on the tin loading. It is also noteworthy that no intermetallic environment (i.e., Sn–Mo, Sn–Co or Sn–Sn) was observed indicating again that tin was linked to the sulfide phases or to the support by way of sulfur (or oxygen) bridges with a high degree of dispersion. The presence of sulfur bridge between tin and cobalt (or molybdenum) could be explained by the fact that the surface of $CoMo/Al_2O_3$ had been saturated by H_2S/H_2 pulses before SOMC treatment (see Section 2). The present characterization results suggest that the hydrogenolysis of tetraallyltin Sn–C bonds took place probably with SH groups and OH groups initially present on $CoMo/Al_2O_3$ sulfide.

EXAFS showed, from the Mo K-edge spectra (Fig. 8) which do not show any sensible change with Sn doping, that the bulk structure of the sulfide phases were not modified by the SOMC treatment as it was previously suggested by XRD, TEM, and electron probe microanalysis (EPMA) [24].

Different locations of doped Sn atoms can now be deduced from IR results, since the various types of sites present on $CoMo/Al_2O_3$ sulfide can be monitored according to different tin loading (Figs. 5 and 7): free OH groups of support (Brønsted sites), Al^{3+} sites of support (Lewis sites), sulfide CUS, and OH groups in H-bonding with sulfide phases (interfacial sites). The introduction of 0.5 wt.% Sn decreased the numbers of OH groups, Al^{3+} sites and sulfide CUS (Figs. 5b and 6). Higher Sn loadings (1.6 or 2.4 wt.% Sn) continued to decrease the number of sulfide CUS but the decreasing rate was considerably lowered. On the other hand, the number of free OH groups and Al^{3+} sites did not change any more at 1.6 or 2.4 wt.% Sn. Some increase in Lewis acid sites could be explained by the formation of Sn^{4+} sites [52]. The decrease of H-bonded OH groups is more pronounced for the highest Sn amount. The site blocking by tin seems to proceed without significant strength change of residual sites, as no evident band shift trend was observed (Fig. 5a). The small decrease in wave number for the samples with 1.6 or 2.4 wt.% Sn could result from specific poisoning of certain sites of sulfide phases or electronic effect, but clear explanation is not possible with the results of present study. Concerning the interfacial sites, a small increase of the band intensity was observed at 0.5 wt.% Sn but higher Sn loadings progressively poison this type of sites (Fig. 7). The information obtained by IR can be summarized as follows: at low Sn loading SOMC preferentially blocked sulfide CUS and some of support sites (free OH groups and Al^{3+} sites) without changing drastically electronic properties, and for higher Sn loadings, then H-bonded and interfacial OH groups started to be poisoned.

4.2. Reaction networks

It is generally suggested that hydrodesulfurization of thiophenic compounds can occur via two alternative pathways: hydrogenation step of thiophene ring followed by S–C bond breaking or direct S–C bond cleavage without pre-hydrogenation. However, different points of view exist about the relative importance of the two pathways, and arguments favoring one of the pathways were often supported by the detection or not of hydrogenated intermediates [7]. In the case of methylthiophene HDS at elevated H_2 pressure, the pre-hydrogenation pathway seems to be favored [7,53]. The detection in the present work of 3-methyltetrahydrothiophene and thiols corresponding to the first C–S bond breaking appears to support this hypothesis.

The conversion of 2,3-DMB2N to 2,3-DMBN showed a typical behavior of consecutive reactions, as shown in Fig. 10 or proposed in [54]. Indeed, 2,3-DMB2N gave only 2,3-DMB1N at the beginning of the reaction and the concentration of 2,3-DMB1N began to decrease with time. Therefore, 2,3-DMB1N was a reaction intermediate. It is remarkable that ISOM was instant under the reaction conditions used and approached rapidly the equilibrium. When the ratio of 2,3-DMB1N/2,3-DMB2N arrived near the equilibrium value, hydrogenation of 2,3-DMB1N started. Direct hydrogenation of 2,3-DMB2N to 2,3-DMBN seems less probable due to its much lower reactivity compared to 2,3-DMB1N [55]. According to the work done by Maurel on Pt/SiO_2 [55], 2,3-DMB1N is about 500 times more active than 2,3-DMB2N primarily due to the difference in adsorption coefficients. Considering the constant isomer distribution during the reaction, it is evident that the ISOM was not kinetically limited contrary to HYD of 2,3-DMB1N. All this consideration permits to propose a reaction network of 2,3-DMB2N hydrogenation over sulfide catalyst (Fig. 15).

Basically the same reaction scheme was involved in 1-hexene HYD (Fig. 12). Isomerization of H1N started during the feed heating under N_2 and near equilibrium composition of isomers was rapidly established. Moreover, the formation of HN from hydrogenation was continually accompanied by this equilibrated isomer distribution. One major difference, compared to 2,3-DMB2N conversion, was that HYD took place readily at the beginning of the reaction, due to the higher reactivity of H1N than those of its isomers with internal double-bond [55]. From these observations, Fig. 16 proposes the global network of H1N conversion, consisting of the H1N isomerization and hydrogenation according to parallel pathways. Even though H2N and H3N isomers were probably not reaction intermediates considering their lower reactivity than their terminal double-bond counterpart [55], the isomer concentration presented a maximum during the reaction (Fig. 12a) due to the reversibility of the reaction [54].

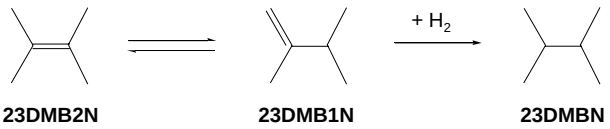

Fig. 15. Proposed reaction network of 2,3-dimethyl-2-butene conversion at 473 K and under total pressure of 2.5 MPa. Feed composition: 10 wt.% 2,3-dimethyl-2-butene, 1000 ppm S as 3-methylthiophene and *n*-heptane.

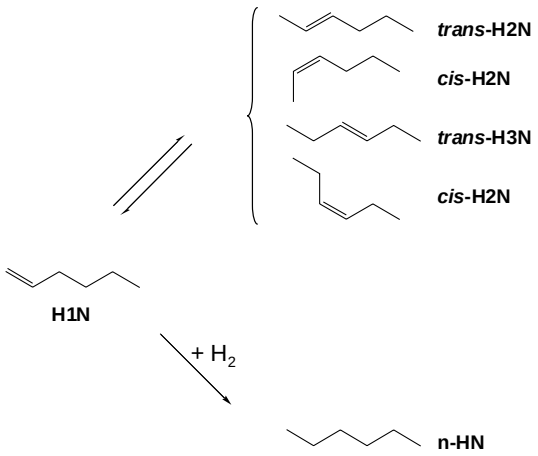

Fig. 16. Proposed reaction network of 1-hexene conversion at 473 K and under total pressure of 2.5 MPa. Feed composition: 10 wt.% 1-hexene, 1000 ppm S as 3-methylthiophene and *n*-heptane.

4.3. Hydrodesulfurization, isomerization and hydrogenation mechanisms

The previous part reported that the various types of sites could be blocked by Sn according to the Sn content: coordinately unsaturated sites on sulfide phases (CUS or sulfur vacancies), free OH groups, H-bonded OH groups, Al^{3+} sites on the support, and finally interfacial sites consisting of support OH groups H-bonded with the sulfide phase. Most significant site blocking concerned sulfide CUS and interfacial sites. The comparison of these results on site number evolution with the activity variation according to tin loading (Figs. 13 and 14) provides important information on the nature of active sites for ISOM, HYD and HDS.

Figs. 13 and 14 show clearly that each of ISOM, HYD and HDS reacted differently to the Sn doping and allow to discriminate active site structures for each reaction. First, ISOM indicated no visible change in catalyst performance for the reaction time higher than 1 h in case of H1N even at 2.4 wt.% Sn (Fig. 13). Before attaining equilibrium isomer composition, we can note that initial activity varies for different Sn loading, but no apparent tendency could be obtained with increasing Sn loading. At present, we could not explain the difference of initial isomerization performance. However, sites blocked by tin do not seem to play an important role in olefin ISOM. Especially, the number of sulfide CUS and interfacial sites did not seem to be rate limiting for olefin ISOM, as even the catalyst with the highest Sn content (2.4 wt.%) resulted in no significant activity decrease, whereas the number of sulfide CUS and interfacial sites was very drastically decreased with doping of 2.4 wt.% Sn. On the contrary, the portion of support OH groups and Al^{3+} sites which remains free after Sn deposition, could therefore be the active sites for olefin ISOM. Indeed, the alumina support has already been proposed as an active phase for olefin isomerization, when the surface Brønsted acidity is maintained by a partial pressure of H_2S or the presence of sulfide phase [56]. As ISOM was very rapidly approaching the equilibrated composition, the diminution of only some part of support sites might not be sufficient to visibly diminish the catalytic activity.

Tin doping brought about net activity decrease for both HYD and HDS (Fig. 14). A higher tin loading led to a more important activity drop. However, the profiles of activity decrease were completely different for these two reactions. First, we can note a good parallel between HDS activity (Fig. 14) and the number of sulfide CUS deduced from IR(CO) areas (Fig. 5b). The plot in Fig. 17 confirms indeed an excellent linear correlation between relative HDS activities and relative areas of IR bands for CO/sulfided phase CUS. The sulfur vacancies on sulfide phases played

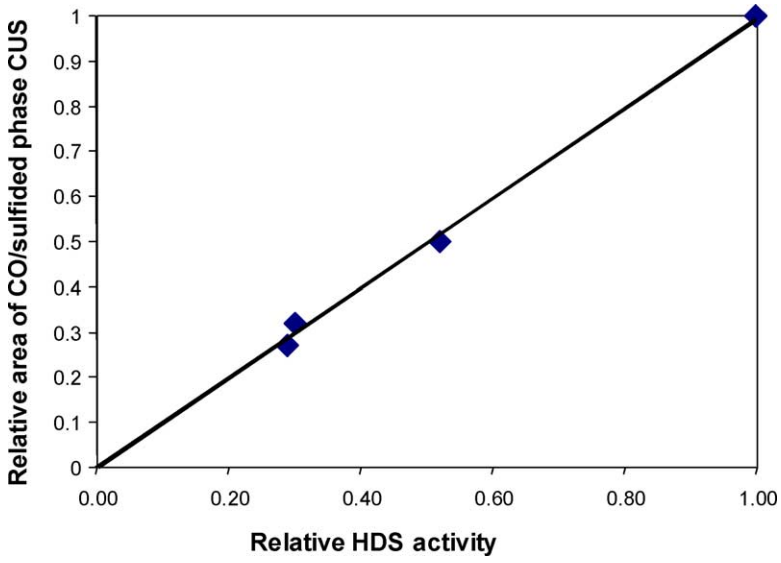

Fig. 17. Linear relationship between HDS activity and the number of sulfided phase CUS.

therefore an important role in HDS catalytic cycle. This finding enters perfectly the generally accepted reaction scheme of HDS over sulfide catalyst, where CUS on sulfide phases are considered as active sites [7].

On the other hand, no evident correlation can be found with CUS, free OH groups or Al^{3+} sites for olefin HYD. The catalyst with 0.5 wt.% Sn showed only a small decrease in HYD, while a sensible diminution of CUS was noted. It indicates that the elementary steps involving sulfur vacancies (olefin or hydrogen activations) were not of primary importance for olefin HYD in our condition of test. In addition, free OH groups and Al^{3+} do not seem to be important in the HYD catalytic cycle either. As, although the number of free OH groups and Al^{3+} sites stayed practically constant for all the Sn-doped catalysts, the activity decrease correlated with the Sn content. Unlike the CUS, hydroxyl groups and Al^{3+} sites, the interfacial sites showed a qualitatively good correspondence with olefin HYD activity. Indeed, a significant diminution of interfacial sites was observed only on the catalysts with 1.6 and 2.4 wt.% Sn and these two catalysts showed lowest HYD activity. The catalyst with 2.4 wt.% Sn had less numerous and less active interfacial sites than the catalyst having 1.6 wt.%. The presence of tin on interfacial sites seems to decrease HYD activity by inhibiting the hydrogen addition to olefin. In this respect, it is noteworthy to reconsider a work done by Candia et al. [26]. As mentioned already, high temperature sulfidation of $CoMo/Al_2O_3$ results in the transition of the active phase from Type I Co–Mo–S structure into Type II Co–Mo–S. This transition is accompanied by thiophene HDS promotion and some inhibition of secondary HYD of butenes. These authors explained this change by more complete sulfidation and diminution of the interaction between sulfide phase and support. Their IR results showed, in effect, the appearance of some free OH groups after high temperature sulfiding, indicating the decrease of interaction with the support. It is interesting to note that the increase of free OH groups is accompanied by a relative decrease of OH groups in interaction with sulfide phases, and thus a decrease of "interfacial sites" according to our terminology.

According to the global picture proposed by the present work, it seems possible to increase HDS/HYD selectivity of the conventional $CoMo/Al_2O_3$ catalysts by addressing different sites: support, interfacial sites and sulfide CUS. The observed discrepancy or poor variation of the selectivity with catalyst modification found in literature (see Section 1) might be due to the difficulty in controlling the catalyst modification. However, further studies are necessary to understand the exact role of interfacial sites in HDS. Also, further investigation is necessary to identify the elementary steps in which interfacial sites are engaged for olefin hydrogenation. One possibility is the participation of this type of sites in the transport of reactant like olefins via the support as proposed in the case of hydrogen for other catalytic systems [57].

5. Conclusions

Tin doping of sulfided $CoMo/Al_2O_3$ by surface organometallic chemistry of tetraallyltin was found to take place keeping the initial morphology of sulfide slabs. Very high tin dispersion seems to have been achieved. Tin complex anchoring was proved to proceed by hydrogenolysis of Sn–C bonds on SH and/or support OH groups. The SH groups might be linked to Mo or Co-promoted Mo sites, H-bonded to support OH groups, or located at Al^{3+} sites. As a result, tin doping led to the blocking of different sites on the sulfide catalysts, depending on tin loading. A small dose of tin blocked preferentially sulfide CUS and some part of support sites (free OH groups and Al^{3+} sites). This site blocking was realized with limited variations of the electronic properties. At higher tin loading, the interfacial sites (made up of support OH groups H-bonded with the sulfide phases) were also poisoned.

The conversion of 3-methylthiophene proceeded via pre-hydrogenation of thiophenic ring and showed an apparent first-order kinetic behavior on $CoMo/Al_2O_3$ sulfides with or without any tin doping. Hydrogenation of 2,3-dimethyl-2-butene was a consecutive reaction involving intermediate isomerization to 2,3-dimethyl-1-butene. Hydrogenation started when equilibrated isomer composition was reached and had apparent zero-order kinetic law. The conversion of 1-hexene involved isomerization and hydrogenation in parallel. The isomer concentration was again quickly equilibrated and hydrogenation followed apparent zero-order kinetic law. No clear correlation could be obtained between tin doping and isomerization performance and the support was proposed to play an important role in this reaction. Tin doping significantly inhibited hydrodesulfurization and olefin hydrogenation. According to infrared spectroscopy and carbon monoxide chemisorption, the decreased hydrodesulfurization activity could be nicely explained by the decreased number of sulfur vacancies on sulfide phases and activity drop in hydrogenation by the disappearance of support hydroxyl groups in interaction with sulfide phases. Sulfur vacancies on sulfide phases were therefore proposed as active sites in hydrodesulfurization, having little impact on olefin hydrogenation or isomerization. The interfacial sites were proposed to play an important role in the olefin hydrogenation pathway, maybe by controlling the transport of the olefin from the support to the sulfide active site.

References

[1] T.G. Kaufmann, A. Kaldor, G.F. Stuntz, M.C. Kerby, L.L. Ansell, Catal. Today 62 (2000) 77.
[2] L.D. Krenzke, J.E. Kennedy, K. Baron, M. Skripek, NPRA Annual Meeting Paper No. AM-96-67, 1996.
[3] R.W. Boubel, D.L. Rox, D.B. Turner, A.C. Stern, Fundamentals of Air Pollution, Academic Press, San Diego, 1994.

[4] F. Baco, Q. Debuisschert, N. Marchal, J.L. Nocca, F. Picard, D. Uzio, Prime G+ process desulfurization of FCC gasoline with minimized octane loss, in: Proceedings of the AIChE Spring National Meeting, New Orleans, March 10–14, 2002.
[5] N.H. Sweed, E.S. Ellis, PTQ Autumn (2001) 45.
[6] S. Hatanaka, M. Yamada, O. Sadakane, Ind. Eng. Chem. Res. 36 (1997) 1519.
[7] H. Topsøe, B.S. Clausen, F.E. Massoth, in: J.R. Anderson, M. Boudart (Ed.), Catalysis, Science and Technology, vol. 11, Springer-Verlag, Berlin, 1996.
[8] J.-L. Nocca, R.M. Gialella, J. Cosyns, J.-P. Burzynski, NPRA Annual Meeting Paper No. AM-95-50, 1995.
[9] L.A. Pine, W.E. Winter, US Patent 4 149 965 (1979), to Exxon.
[10] C. Sudhakar, G.G. Sandford, US Patent 5 286 373 (1994), to Texaco.
[11] O. Sadakane, Y. Sasaki, R. Ohnishi, EP Patent 0 745 660 (2000), to Mitsubishi.
[12] S. Hatanaka, M. Yamada, O. Sadakane, Ind. Eng. Chem. Res. 37 (1998) 1748.
[13] S. Hatanaka, O. Sadakane, EP Patent 0 905 214 (1999), to Mitsubishi.
[14] S. Hatanaka, O. Sadakane, H. Okazaki, Sekiyu Gakkaishi 44 (2001) 36.
[15] A.P. Yu, E.C. Myers, US Patent 4 132 632 (1979), to Standard Oil.
[16] C. Sudhakar, US Patent 5 770 046 (1998), to Texaco.
[17] J.T. Miller, W.J. Reagan, J.A. Kaduk, C.L. Marshall, A.J. Kropf, J. Catal. 193 (2000) 123.
[18] S. Kasztelan, H. Toulhoat, J. Grimblot, J.P. Bonnelle, Appl. Catal. 13 (1984) 127.
[19] H. Topsøe, B.S. Clausen, Catal. Rev.-Sci. Eng. 26 (1984) 395.
[20] R. Prins, V.H.J. de Beer, G.A. Somorjai, Catal. Rev.-Sci. Eng. 31 (1989) 1.
[21] F. Maugé, A. Vallet, J. Bachelier, J.C. Duchet, J.C. Lavalley, Catal. Lett. 2 (1989) 57.
[22] K. Inamura, R. Prins, Stud. Surf. Sci. Catal. 92 (1995) 401.
[23] S. Hatanaka, M. Yamada, O. Sadakane, Ind. Eng. Chem. Res. 36 (1997) 5110.
[24] J.-S. Choi, C. Petit-Clair, D. Uzio, Stud. Surf. Sci. Catal. 143 (2002) 585.
[25] C.N. Satterfield, G.W. Roberts, AIChE J. 14 (1968) 159.
[26] R. Candia, O. Sørensen, J. Villadsen, N.-Y. Topsøe, B.S. Clausen, H. Topsøe, Bull. Soc. Chim. Belg. 93 (1984) 763.
[27] J.P. Candy, B. Didillon, E.L. Smith, T.B. Shay, J.M. Basset, J. Mol. Catal. 86 (1994) 179.
[28] J.P. Candy, O.A. Ferretti, G. Mabilon, J.P. Bournonville, A. El Mansour, J.M. Basset, G. Martino, J. Catal. 112 (1988) 210.
[29] B. Didillon, C. Houtman, T. Shay, J.P. Candy, J.M. Basset, J. Am. Chem. Soc. 115 (1993) 9380.
[30] F. Humblot, B. Didillon, F. Le Peltier, J.P. Candy, J. Corker, O. Clause, F. Bayard, J.M. Basset, J. Am. Chem. Soc. 120 (1998) 137.
[31] F. Maugé, J.C. Lavalley, J. Catal. 137 (1992) 69.
[32] Y.I. Yermakov, A.N. Startsev, V.A. Burmistrov, Appl. Catal. 11 (1984) 1.
[33] M. Angulo, F. Maugé, J.C. Duchet, J.C. Lavalley, Bull. Soc. Chim. Belg. 96 (1987) 925.
[34] T.R. Halbert, T.C. Ho, E.I. Stiefel, R.R. Chianelli, M. Daage, J. Catal. 130 (1991) 116.
[35] W. Kündig, Nucl. Instrum. Meth. 75 (1969) 336.
[36] D.E. Sayers, B.A. Bunker, in: D.C. Koningsberger, R. Prins (Eds.), X-ray Absorption: Principles, Applications, Techniques of EXAFS, SEXAFS and XANES, Wiley, New York, 1998, p. 211.
[37] A. Michalowicz, Ph.D. Thesis, University of Val de Marne, France, 1990.
[38] A.L. Ankudinov, B. Ravel, J.J. Rehr, S.D. Conradson, Phys. Rev. B 58 (1998) 7565.
[39] J. Bachelier, M.J. Tilliette, M. Cornac, J.C. Duchet, J.C. Lavalley, D. Cornet, Bull. Soc. Chim. Belg. 93 (1984) 743.
[40] M.I. Zaki, H. Knözinger, Mater. Chem. Phys. 17 (1987) 201.
[41] B. Müller, A.D. van Langeveld, J.A. Moulijn, H. Knözinger, J. Phys. Chem. 97 (1993) 9028.
[42] G. Della Gatta, B. Fubini, G. Ghiotti, C. Morterra, J. Catal. 43 (1976) 90.
[43] J.B. Peri, J. Phys. Chem. 86 (1982) 1615.
[44] M.I. Zaki, B. Vielhaber, H. Knözinger, J. Phys. Chem. 90 (1986) 3176.
[45] N.-Y. Topsøe, J. Catal. 64 (1980) 235.
[46] N.-Y. Topsøe, H. Topsøe, J. Catal. 139 (1993) 631.
[47] N.-Y. Topsøe, H. Topsøe, J. Catal. 139 (1993) 641.
[48] H. Topsøe, B.S. Clausen, N.-Y. Topsøe, J.K. Nørskov, C.V. Ovesen, C.J.H. Jacobsen, Bull. Soc. Chim. Belg. 104 (1995) 283.
[49] S.M.A.M. Bouwens, R. Prins, V.H.J. de Beer, D.C. Koningsberger, J. Phys. Chem. 94 (1990) 3711.
[50] S.M.A.M. Bouwens, J.A.R. van Veen, D.C. Koningsberger, V.H.J. de Beer, R. Prins, J. Phys. Chem. 95 (1991) 123.
[51] J.T. Miller, C.L. Marshall, A.J. Kropf, J. Catal. 202 (2001) 89.
[52] N. Sergent, P. Gélin, L. Périer-Camby, H. Praliaud, G. Thomas, Phys. Chem. Chem. Phys. 4 (2002) 4802.
[53] H. Schulz, M. Schon, N.M. Rahman, Stud. Surf. Sci. Catal. 27 (1986) 201.
[54] J.C. Jungers, J.C. Balacéanu, F. Coussemant, F. Eschard, A. Giraud, M. Hellin, P. Leprince, G.E. Limido, Cinétique Chimique Appliquée, Technip, Paris, 1958.
[55] R. Maurel, in: B. Claudel (Ed.), La Catalyse au Laboratoire et dans l'Industrie, Masson, Paris, 1967, p. 203.
[56] S. Karmal, G. Pérot, D. Duprez, J. Catal. 130 (1991) 212.
[57] R. Prins, Stud. Surf. Sci. Catal. 138 (2001) 1.